ChemPubSoc Europe

DOI: 10.1002/cssc.201801255

CHEMSUSCHEM Full Papers

Panchromatic Sensitization with Zn^{II} Porphyrin-Based Photosensitizers for Light-Driven Hydrogen Production

Po-Yu Ho[+],[a] Michael F. Mark[+],[b] Yi Wang,[a] Sze-Chun Yiu,[a] Wai-Hong Yu,[a] Cheuk-Lam Ho,*[a] David W. McCamant,*[b] Richard Eisenberg,[b] and Shuping Huang*[c]

Three molecular photosensitizers (PSs) with carboxylic acid anchors for attachment to platinized titanium dioxide nanoparticles were studied for light-driven hydrogen production from a fully aqueous medium with ascorbic acid (AA) as the sacrificial electron donor. Two zinc(II) porphyrin (ZnP)-based PSs were used to examine the effect of panchromatic sensitization on the photocatalytic H_2 generation. A dyad molecular design was used to construct a difluoro boron-dipyrromethene (bodipy)-conjugated ZnP PS (ZnP-dyad), whereas the other one featured an electron-donating diarylamino moiety (YD2-*o*-C8). To probe the use of the ZnP scaffold in this particular energy conversion process, an organic PS without the ZnP moiety (Bodipy-dye) was also synthesized for comparison. Ultrafast transient absorption spectroscopy was adopted to map out the energy transfer processes occurring in the dyad and to establish the bodipy-based antenna effect. In particular, the systems with YD2-*o*-C8 and ZnP-dyad achieved a remarkable initial activity for the production of H_2 with an initial turnover frequency (TOF_i) higher than 300 h^{-1} under white light irradiation. The use of ZnP PSs in dye-sensitized photocatalysis for the H_2 evolution reaction in this study indicated the importance of the panchromatic sensitization capability for the development of light absorbing PSs.

Introduction

Energy is probably one of the most critical factors that will shape our society in the 21st century.[1] Scientists and engineers are making efforts to improve the accessibility of sustainable energy resources because excessive burning of fossil fuel will result in local air pollution problems and global climate change.[2] Harnessing solar energy to produce hydrogen fuel from water through the water splitting reaction is a promising method to support sustainable development and exploit alternative energy resources.[3] Hydrogen is considered to be an ideal energy carrier with no carbon footprint; it can be generated from water, so there is a tremendous amount of feedstock freely provided by mother nature.[4] In addition, H_2 fuel can be utilized as a reagent to produce other important industrial chemicals, such as methane and methanol.[5]

The water splitting reaction is a key energy-storage reaction that consists of two redox half reactions: i) reduction of two aqueous protons to one H_2 at the cathodic side and ii) oxidation of two water molecules to one O_2 molecule at the anodic side.[6] In this study, we focused on the reductive side of water splitting, concentrating our efforts on the photocatalytic generation of H_2 in its simplest form, which requires a photosensitizer (PS) for exciton formation, a pathway for charge separation, a catalyst for the conversion of two aqueous protons into a hydrogen molecule, and a source of electrons (i.e., a sacrificial electron donor).[7]

In the past few decades, metal-complex-based PSs that absorb visible light have been widely investigated for water reduction. Most of these PSs contain noble metals such as ruthenium(II), iridium(III), and platinum(II) metal centers.[7,8] However, these charge-transfer complexes typically suffer from inefficient photon capture because of their poor absorption in the blue–green region of the spectrum and low molar absorptivities ($\approx 7–15\times10^3\ M^{-1}\,cm^{-1}$).[9] In 2015, Zheng et al. reported new dyads consisting of a strongly absorbing difluoro boron-dipyrromethene (bodipy) and a platinum diimine dithiolate (PtN_2S_2) chromophore, which, when grafted onto platinized TiO_2 nanoparticles (TiO_2–Pt), showed much greater efficiency for the harvesting of photons at 530 nm than the PtN_2S_2 chromophores alone.[10] This dyad approach improved upon the aforementioned drawbacks of noble metal charge-transfer complexes.

[a] *Dr. P.-Y. Ho,[+] Y. Wang, Dr. S.-C. Yiu, W.-H. Yu, Dr. C.-L. Ho*
Department of Applied Biology and Chemical Technology
The Hong Kong Polytechnic University
Hong Hom, Hong Kong (P. R. China)
E-mail: cheuk-lam.ho@polyu.edu.hk

[b] *M. F. Mark,[+] Dr. D. W. McCamant, Prof. R. Eisenberg*
Department of Chemistry
University of Rochester
Rochester, New York 14627 (United States)
E-mail: mccamant@chem.rochester.edu

[c] *Dr. S. Huang*
College of Chemistry
Fuzhou University
Fuzhou, Fujian 350108 (P. R. China)
E-mail: huangshp@gmail.com

[+] *These authors contributed equally to this work.*

Supporting Information and the ORCID identification number(s) for the author(s) of this article can be found under: https://doi.org/10.1002/cssc.201801255.

It is of significant interest to develop a new category of noble-metal-free dyes with strong and panchromatic sensitization properties for the generation of H_2. In nature, porphyrin and its derivatives are the chromophores adopted as solar photosynthetic cores in plants and bacteria.[11] In general, free-base and metallated porphyrin absorption spectra are characterized by strong Soret band(s) absorbing blue light ($\varepsilon > 10^5\,M^{-1}\,cm^{-1}$; approximately 400 nm) and Q bands centered between 500–700 nm ($\varepsilon > 10^4\,M^{-1}\,cm^{-1}$).[12] Because of this attractive dual-absorption band feature, ZnP derivatives have been extensively investigated for use in dye-sensitized solar cells (DSSCs).[11a] Yeh et al. made a significant contribution to the development of DSSCs by optimizing ZnP-based dyes; they also found the electronic push–pull effect had a large impact on the power conversion efficiency (PCE).[13] In 2011 and 2012, alkoxy-wrapped push–pull ZnP dyes were reported to achieve PCEs >8% in the corresponding DSSCs, and the long alkoxy chains in the *ortho*-positions of the *meso*-phenyl groups on the porphyrin scaffold reduced dye aggregation and boosted the charge collection yield.[14] Nevertheless, studies exploiting molecular engineered ZnP PSs for light-driven production of hydrogen based on PS–TiO_2–Pt hybrid material remain scarce.

In 2010, Lee and Hupp synthesized a new molecular dyad containing a bodipy organic chromophore covalently linked to ZnP through a phenyl-ethynyl linkage; the dyad showed increased photon-to-current conversion efficiency in a DSSC.[15] Although this chromophore showed improved DSSC efficiency, it has not yet been utilized as a PS for hydrogen production, and the ultrafast dynamics associated with the energy transfer events in the dyad have not been characterized. In this work, we utilized a similar molecular dyad, ZnP-dyad, which contained small changes in the aliphatic tails, as a PS for the solar-energy production of hydrogen and fully characterized the bodipy to ZnP energy transfer dynamics.

Herein, we describe a light-driven hydrogen production study utilizing three different anchor-containing PSs (Figure 1) and the corresponding PS–TiO_2–Pt composite materials. One of the PSs YD2-*o*-C8 (a highly efficient ZnP dye for DSSCs first reported in 2011[14a,b]) was systematically compared with the designed bodipy-conjugated ZnP dye (ZnP-dyad). Ultrafast transient absorption spectroscopy was used to study the energy transfer processes initiated from the different excited states of ZnP-dyad (shown in Scheme 1). Furthermore, an organic PS containing a bodipy unit (Bodipy-dye) was synthesized to compare the light-harvesting effects attributed to the ZnP unit. In addition, because the ZnP-dyad and YD2-*o*-C8 were both panchromatic in nature, both green and white lights were used to examine the significance of the panchromatic sensitization as well as the effect of the molecular design of the dyad. The results revealed a number of factors that should be considered for designing an ideal molecular PS for light-driven hydrogen generation from aqueous media.

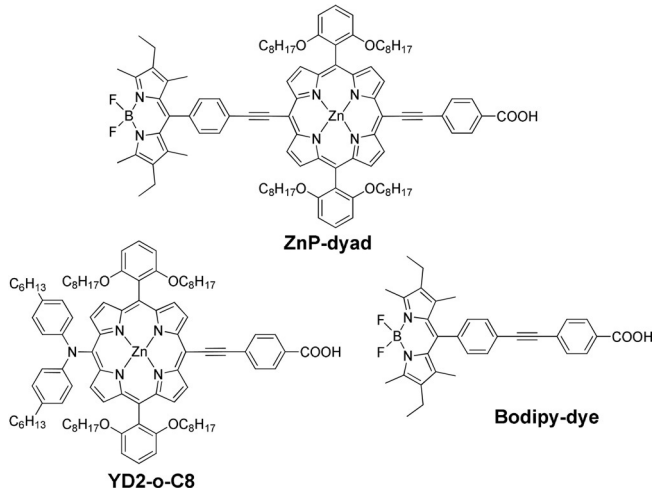

Figure 1. Chemical structures of PSs ZnP-dyad, YD2-*o*-C8, and Bodipy-dye.

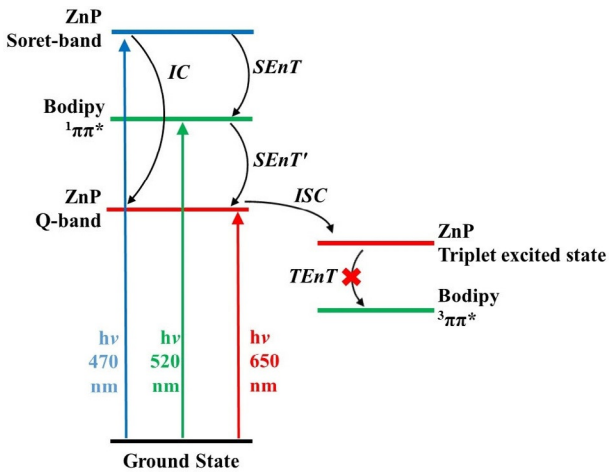

Scheme 1. Possible processes involved upon excitation of ZnP-dyad (SEnT = singlet energy transfer, IC = internal conversion, ISC = intersystem crossing, and TEnT = triplet energy transfer).

Results and Discussion

Synthesis and characterization

The synthetic routes for the synthesis of ZnP-dyad and Bodipy-dye are shown in Scheme 2. The key intermediates, iodo-compound (1) and a triisopropylsilane (TIPS)-protected diethynyl Zn^{II} porphyrin (ZnP) were synthesized according to the reported procedures.[15,16] The pure organic molecule Bodipy-dye was prepared by Sonogashira coupling of 4-iodobenzoic acid (≈80% yield) with bodipy-based compound **3** containing an ethynyl group. For the bodipy-conjugated ZnP dyad, deprotection of the ethynyl groups using tetra-*n*-butylammonium fluoride and further unsymmetrical Sonogashira coupling with 4-iodobenzoic acid and compound 1 rendered the corresponding product ZnP-dyad in approximately 50% yield. All the intermediates and target compounds were purified by column chromatography on silica gel and fully characterized by ^1H and ^{13}C NMR spectroscopy and matrix-assisted laser desorption ionization time-of-flight (MALDI-TOF) mass spectrometry.

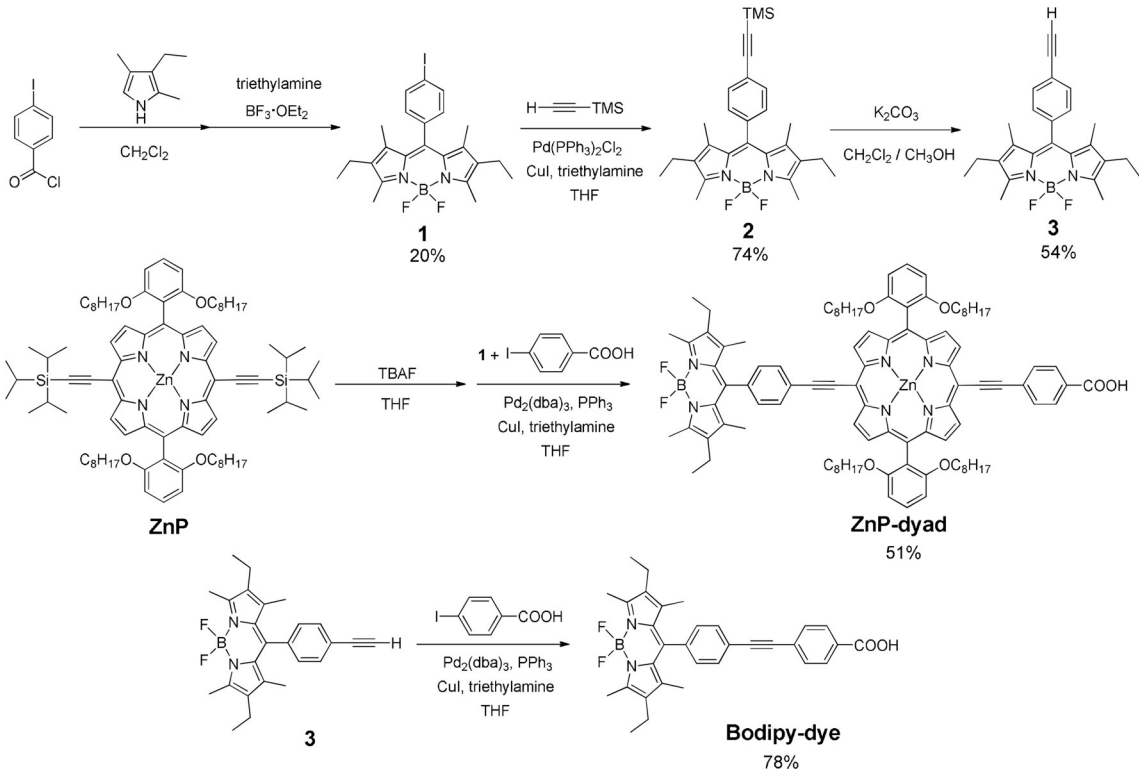

Scheme 2. Synthetic routes for ZnP-dyad and Bodipy-dye.

Photophysical properties

The photophysical properties of ZnP-dyad, YD2-*o*-C8, and Bodipy-dye were studied in CH_2Cl_2 solutions at ambient temperature. Their UV/Vis absorption spectra and emission spectra are shown in Figure 2 and S11, respectively, and the corresponding data are tabulated in Table 1. The organic PS Bodipy-dye had similar characteristics to that of typical bodipy chromophores in both the absorption and fluorescence spectra. A sharp band at 526 nm was observed in the absorption spectrum and an emission peak was observed at 544 nm, both owing to the $S_0 \rightarrow S_1$ ($^1\pi\pi^*$) transition.[17] The absorption spectrum of YD2-*o*-C8 featured an intense Soret band at 441 nm and less-intense Q bands at 577 and 641 nm. After photoexciting of this push–pull ZnP molecule at the Soret-band wavelength, it emitted a single peak at 678 nm owing to Q-band fluorescence. After substituting the diarylamino functional group in YD2-*o*-C8 with an ethynylene-bridged phenyl-bodipy unit, the ZnP-dyad exhibited panchromatic sensitization with an extended absorption onset at 765 nm from the Q bands, a Soret band at 455 nm, the $S_0 \rightarrow S_1$ ($^1\pi\pi^*$) transition from the bodipy moiety at 525 nm, and a sharp Q band at 659 nm. The absorption spectrum of the ZnP-dyad was the sum of the two constituent chromophores, which was similar to those of other bodipy-porphyrin light-harvesting arrays.[18] In addition, an extended shoulder peak among the Q bands was located at 730 nm, which originated from the elongated π-conjugation. Correspondingly, the peak located at the near-infrared region absorbed light beyond the typical metallated porphyrin chromophores. Conversely, this dyad exhibited different photoluminescence spectra when excited at the Soret band or the bodipy-based absorption peak wavelengths. When excited at the Soret-band wavelength, this molecule emitted

Table 1. Absorption and emission data of ZnP-dyad, YD2-*o*-C8, and Bodipy-dye in CH_2Cl_2.

Dye	λ_{abs} [nm] (ε [$M^{-1}cm^{-1}$])	λ_{onset} [nm]	λ_{em} [nm]
ZnP-dyad	455 (281 000), 525 (45 300), 659 (48 100)	765	544, 669, 743
YD2-*o*-C8	441 (167 000), 577 (11 800), 641 (23 300)	685	678
Bodipy-dye	526 (33 700)	544	544

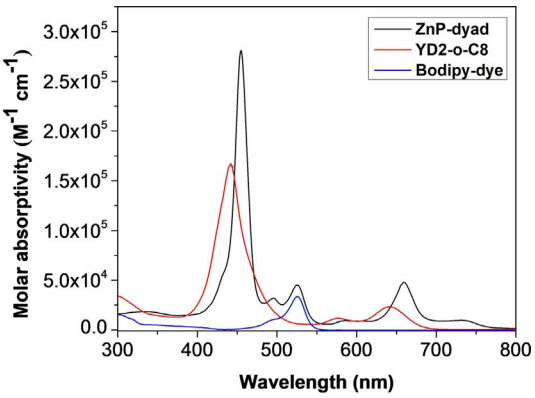

Figure 2. UV/Vis absorption spectra of the PSs ZnP-dyad, YD2-*o*-C8, and Bodipy-dye in CH_2Cl_2 at ambient temperature.

strongly at 669 nm with a shoulder peak at 743 nm, both of which originated from the Q bands. However, when it was excited at the bodipy-based transition, the dyad showed an additional emission peak with a lower intensity at 544 nm. The presence of the Q-band emission following excitation of the bodipy revealed an energy transfer process from the peripheral bodipy chromophore to the core ZnP chromophore, which had an energy transfer rate that was comparable to the radiative lifetime of the bodipy.

Electrochemical properties

Cyclic voltammetry (CV) measurements of these PSs focusing on positive applied potential (0–1.5 V versus SCE) were performed (Table 2). The cyclic voltammogram (Figure 3) of Bodipy-dye exhibited only one reversible oxidative wave ($E_{1/2}$ = 1.08 V), which corresponded to the formation of a bodipy radical cation.[19] The cyclic voltammogram of YD2-*o*-C8 possessed two reversible oxidation peaks ($E_{1/2}$ = 0.54 V and 0.98 V), which both originated from the simultaneous oxidation of the ZnP core and the diarylamino moiety.[13c] The cyclic voltammogram of the ZnP-dyad was the sum of reversible oxidation of the ZnP core ($E_{1/2}$ = 0.83 V) and the bodipy unit ($E_{1/2}$ = 1.09 V).[15]

Table 2. Electrochemical data and energy levels of ZnP-dyad, YD2-*o*-C8, and Bodipy-dye.

Dye	E_{ox}[a] [V]	E_{HOMO}[b] [eV]	$E_{0\text{-}0}$[c] [eV]	E_{ox^*}[d] [V]	E_{LUMO}[e] [eV]
ZnP-dyad	0.72	−5.14	1.62	−0.90	−3.52
YD2-*o*-C8	0.50	−4.92	1.81	−1.31	−3.11
Bodipy-dye	1.00	−5.42	2.28	−1.28	−3.14

[a] Half-wave oxidation potentials were measured by cyclic voltammetry in dry CH_2Cl_2 solution containing 0.1 M $[NBu_4][PF_6]$ as the supporting electrolyte (versus the SCE reference electrode). Under these conditions, the reversible oxidation of ferrocene was $E_{1/2}$ = 0.38 V. [b] Calculated from (E_{ox} + 4.42), because the E_{HOMO} of ferrocene is equal to −4.80 eV versus vacuum level. [c] $E_{0\text{-}0}$ was determined from the onset of the absorption spectrum. [d] $E_{ox^*} = E_{ox} - E_{0\text{-}0}$. [e] $E_{LUMO} = E_{HOMO} + E_{0\text{-}0}$.

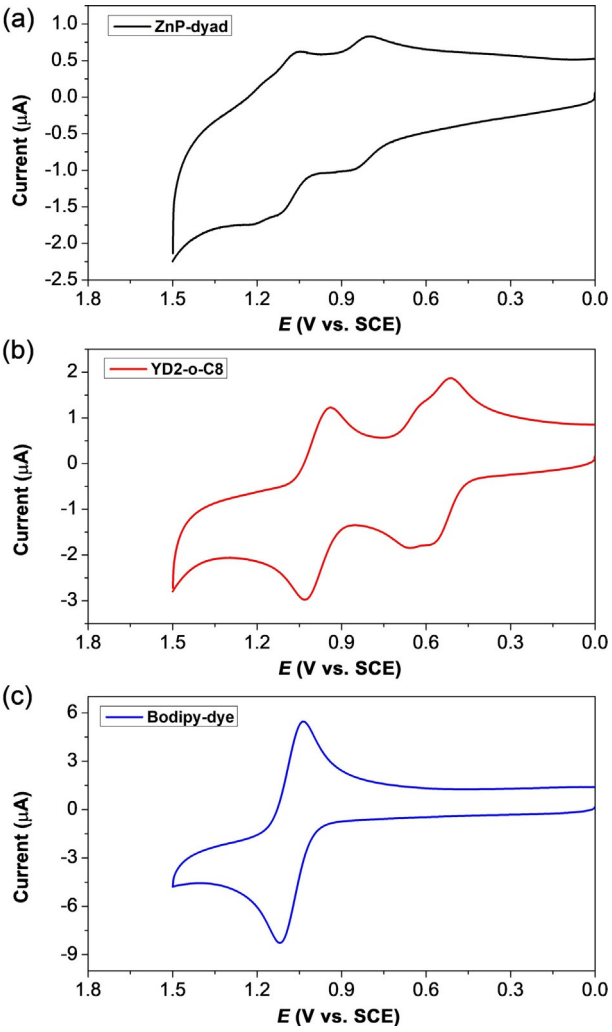

Figure 3. Cyclic voltammograms of (a) ZnP-dyad, (b) YD2-*o*-C8, and (c) Bodipy-dye in dry CH_2Cl_2 with 0.1 M tetrabutylammonium hexafluorophosphate as supporting electrolyte at a scan rate of 0.1 $V s^{-1}$.

As shown in Table 2, the E_{HOMO} of these PSs (−4.92 to −5.42 eV, relative to vacuum) were all more negative than the redox potential energy level (−4.65 eV, pH ≈ 4) of ascorbic acid[20] (AA; as the sacrificial electron donor in the H_2 production experiment) and the corresponding E_{LUMO} (−3.11 to −3.52 eV) were all higher than the conduction band energy level (≈ −4.26 eV) of titanium dioxide nanoparticles.[21] Therefore, effective dye regeneration[22] and electron injection[23] were both expected to proceed in the photocatalytic H_2 generation cycle.

Computational studies

The ground state geometries of these PSs were optimized using density functional theory (DFT) calculations (Figure 4, S13 and S14) and the dihedral angles between neighboring units are shown in Figure 5. The electron density in the HOMO and LUMO of Bodipy-dye was localized at the bodipy unit, whereas the anchor moiety was perpendicular to the plane of bodipy unit and the π-conjugation was disconnected at the twist point. The electron density of YD2-*o*-C8 was distributed into the π-conjugation system of the ZnP core and diarylamino moiety in the HOMO, whereas the electron density in the LUMO was mainly located in the ZnP core and phenylethynylene unit. This HOMO and LUMO configuration was anticipated to result in a prominent intramolecular charge-transfer (ICT) character for the excited dye, explaining the origin of the push–pull character in the ZnP dye.[24] The electron density of the ZnP-dyad in the HOMO and LUMO was distributed primarily in the ZnP core and two phenylethynylene units, respectively. Notably, the plane of the ZnP core was not coplanar with the two phenylethynylene units or with the plane of the bodipy unit; hence the direct communication of the π-electron density between ZnP core and bodipy unit was expected to be insignificant.

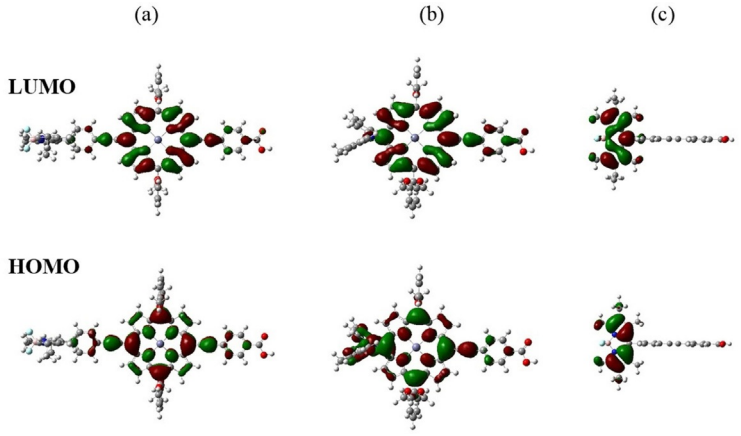

Figure 4. Selected molecular orbital diagrams for (a) ZnP-dyad, (b) YD2-*o*-C8, and (c) Bodipy-dye obtained by DFT calculations with LC-wPBE. To simplify the calculations, alkyl chains on the photosensitizers were replaced with methyl groups.

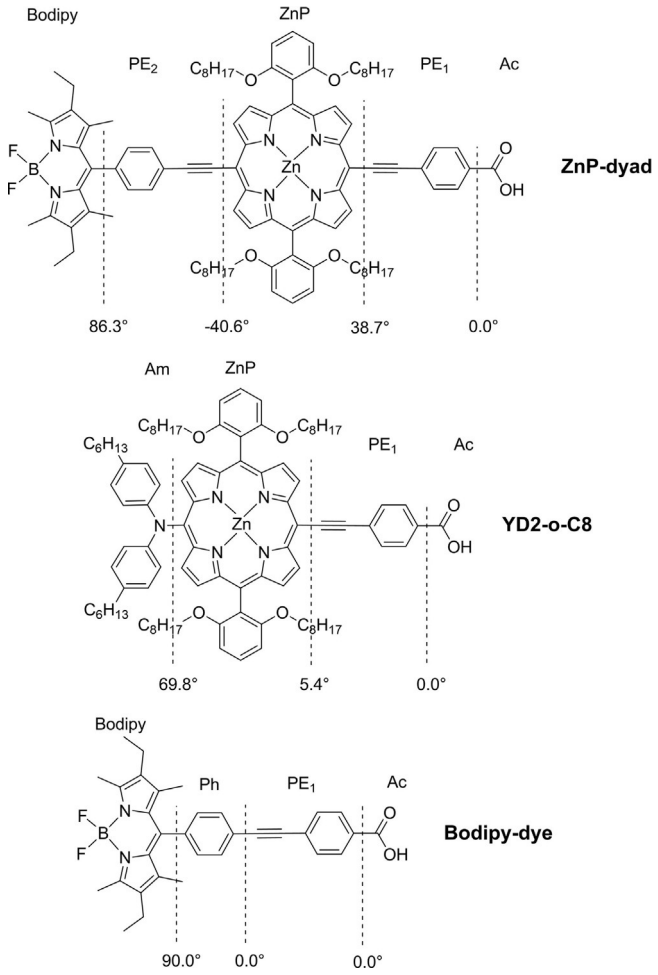

Figure 5. Dihedral angles between the neighboring units or between the phenylethynylene moiety and the carboxylic acid in ZnP-dyad, YD2-*o*-C8, and Bodipy-dye, as determined by DFT geometry optimizations.

Transient absorption

Femtosecond transient absorption (TA) control experiments of Bodipy-dye (Figure S17) and YD2-*o*-C8[25] confirmed prior observations of their excited state spectra and dynamics. The Bodipy-dye exhibited transient signals that decayed slowly with the $^1\pi\pi^*$'s 5–7 ns excited state lifetime, controlled by radiative and nonradiative internal conversion to the ground state.

The TA spectra of the ZnP-dyad at each of the excitation wavelengths are shown in Figure 6. To fully map out the relaxation dynamics of the ZnP-dyad, each of the three absorption bands (Figure 6a) were selectively probed through excitation at 650, 520, and 470 nm (Figure 6b, 6c and 6d). Common to all the spectra, the ground state bleach (GSB) of both the Soret and Q bands were observed at 456 and 658 nm, respectively. A very broad excited state absorption (ESA) from 468 nm into the near-IR was immediately present upon excitation of either of the porphyrin absorption bands. That broad ESA changed shape upon relaxation from the Soret state (the porphyrin S_2) into the Q-band state (the porphyrin S_1) and again at long times following intersystem crossing (ISC) to the triplet manifold. None of the transient spectra returned to zero owing to formation of a long-lived triplet state; however, all spectra retained a similar shape at long times, showing that regardless of the excitation wavelength the molecule ended up in the same state: the T_1 state on the porphyrin. From the longtime decay kinetics, the lifetime of the lowest energy excited singlet was 1300 ± 200 ps (see Figure S18), indicating a 0.77 ns^{-1} ISC rate.

Excitation with a 650 nm pump pulse was used to selectively excite the Q band with a λ_{max} of 658 nm. This approach avoided populating the excited states of both the porphyrin S_2 transition (Soret band) and the bodipy antenna, allowing for the observation of the dynamics associated only with the lowest energy transition. As shown in Figure 6b and 7a, immediately following excitation, bleaches were apparent, which mirrored the ground-state absorption of both the Soret- and Q-band transitions. There was also an instantaneous appearance of a broad ESA that extended throughout the probed spectral window, interrupted only by the porphyrin ground-state bleaches. Within the first 100–300 fs, the bleaches at 458 and 665 nm displayed a loss in amplitude, whereas at 478 nm, the λ_{max} of the ESA, the signal rapidly decayed with a 160 fs time constant. We attributed each of these 100–300 fs processes to ultrafast intramolecular reorganization of the excited state, combined with some degree of solvent reorganization. This reorganization was in agreement with the kinetics of the redshift of the negative signal at the Q-band wavelengths, because ultrafast reorganization produced a minor Stokes shift in the Q-band-stimulated emission. Following the ultrashort time dynamics, a third time constant of approximately 2 ps with an extremely small amplitude was attributed to vibrational relaxation within hot S_1, as seen by the narrowing and redshift of the Q band and lack of any dynamics associated with the Soret bleach. The small amplitude associated with this time constant was owing to excitation near E_{00} of the Q band resulting in only a small vibrationally excited population. Similar kinetics were observed across the entire spectrum as the ESA ex-

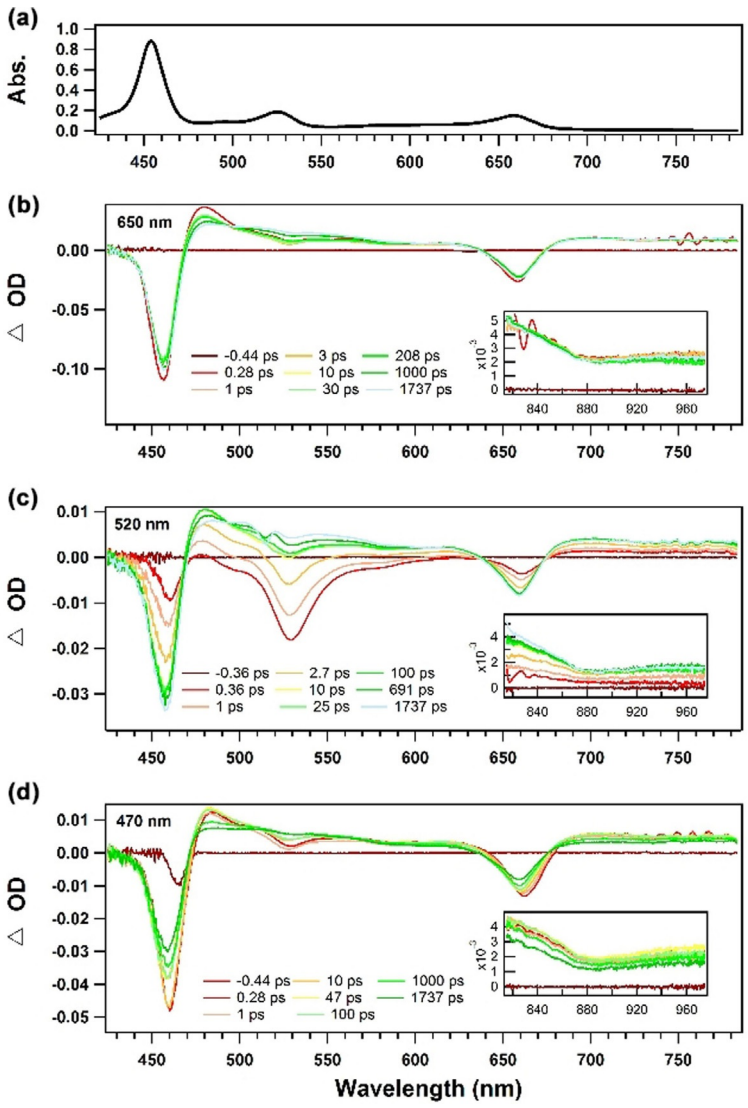

Figure 6. (a) The ground-state absorption spectrum of ZnP-dyad in THF with the transient femtosecond transient absorption spectra with excitation at (b) 650 nm, (c) 520 nm and (d) 470 nm. NIR data is presented in the insets for each of the experiments.

tended to the NIR. A similar value of 2–6 ps has been reported by di Nunzio et al. for the similar YD2-*o*-C8 PS.[25] Lastly, we observed a loss of amplitude in the 478 nm shoulder of the ESA with a 1300 ps time constant, indicating that the molecule underwent ISC to the triplet manifold, which then persisted past the duration of the experiment.

A 520 nm pump pulse was used to selectively excite the bodipy moiety separately from the porphyrin bands (Figure 6c). Following laser excitation, an immediate bleach was formed centered at 527 nm, similar to that of excitation of the Bodipy-dye, as shown in Figure S17. At early times, a slight ultrafast (300–500 fs) attenuation was seen at wavelengths of 478 and 527 nm, characteristic of vibrational cooling of the bodipy moiety. Following this process, the bleach at 527 nm lost all its amplitude with a 2.3 ps time constant, whereas both the Soret- and Q-band bleaches appeared with similar time constants. ESA to the red region of the Q-band bleach, and in the near-IR (inset of Figure 6c), which was attributed to the ESA from the Q-band population, increased in amplitude as the Q-band bleach formed. As shown in Figure 7b, the signal was dominated by the large amplitude associated with this time constant, which we attributed to efficient energy transfer from the bodipy to the porphyrin moiety in 2.3 ps. Interestingly, vibrational relaxation (VR) of the excited porphyrin following the energy transfer was not observed because VR occurs at the same rate or slightly faster than the energy transfer.

To determine if energy transfer was possible from the Soret band into the bodipy moiety, excitation of the S_2 transition was accomplished with a pump pulse of 470 nm overlapping with the red-edge of the Soret band. Immediately following excitation, bleaches at the Soret and Q bands were formed with a minor bleach of the bodipy formed at 527 nm. By quantifying each of these signals over the first approximately 10 ps (see details in the Supporting Information), we determined that 94% of the pump pulse absorption occurred in the Soret band and only 6% of the pump-induced absorptions excited the bodipy directly.

In the spectra and kinetics before 500 fs, slight decreases in the amplitude of the Soret and Q-band bleaches are observed, concurrent with an increase of the bleach at 527 nm, all of which occur with an average time constant of 280 fs. We assigned this to energy transfer from the higher energy Soret band to the bodipy moiety occurring at the same time as internal conversion from the Soret band to the Q band. Quantification of these dynamics are provided in the Supporting Information and show that within 300 fs, 87% of the excited Soret population undergoes internal conversion (IC) to the Q band and 13% undergoes energy transfer into the bodipy moiety. In the subsequent approximately 2.5 ps, the blue light side of the spectrum showed an increase in bleach of the Soret band, whereas a loss was observed at the shoulder of the ESA centered at 478 nm. Within this same time period, the growth of a new broadly absorbing ESA was observed, which covered most of the spectrum, and a loss in bleach amplitude of the Q band occurred. The loss of signal at 478 nm was attributed to loss of the Soret to S_n transition, whereas the loss in bleach at 665 nm was the result of the overlap with the Q-band bleach and the newly formed absorption of the $S_1 \rightarrow S_n$ state. We attributed the shorter time constant ($\approx$100 fs) to simultaneous internal conversion from the Soret to the Q band and energy transfer from the Soret band to bodipy, and we attributed the longer time constant ($\approx$2.5 ps) to energy transfer from the excited bodipy to the Q band.

Lastly, there was no evidence of triplet energy transfer (TEnT) from the ZnP to the bodipy at any excitation wavelength, which would be visible in a long-term bleach of the bodipy absorption band. This indicated that the orbitals localized on either portion of the dyad were well insulated from

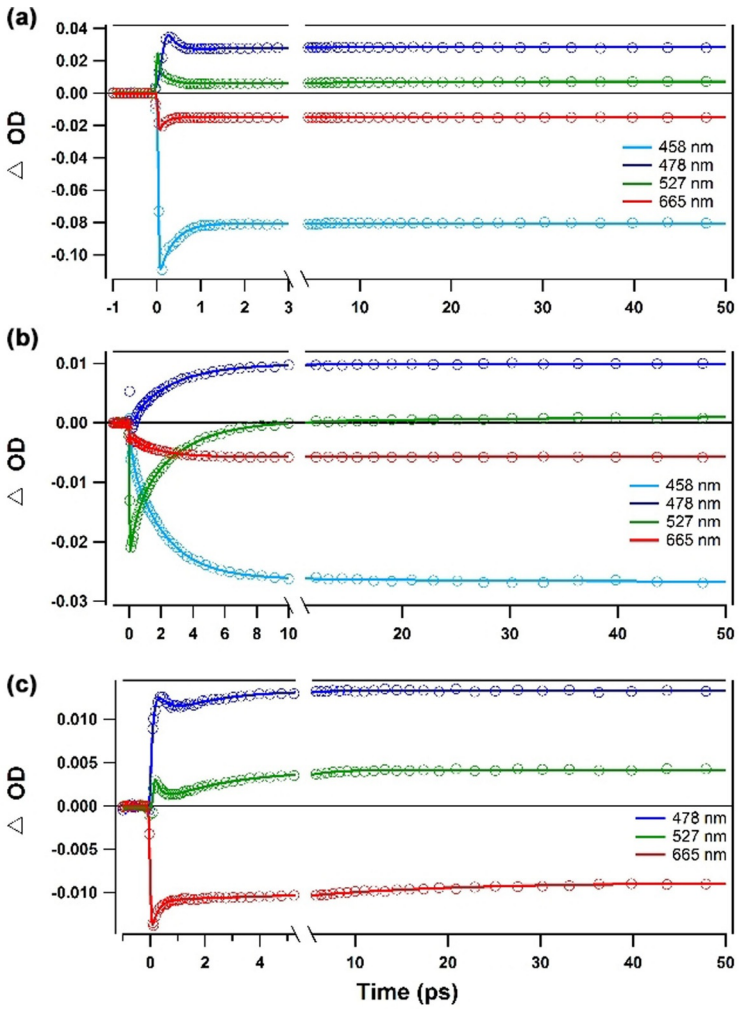

Figure 7. Kinetic fits of transient absorption signals of ZnP-dyad with excitation at (a) 650 nm, (b) 520 nm and (c) 470 nm.

each other, providing no orbital overlap necessary for TEnT. However, we could not rule out the occurrence of TEnT on timescales much longer than the 2 ns TA experiment.

Photocatalytic hydrogen generation

In view of the panchromatic light-absorbing properties of ZnP-dyad and YD2-*o*-C8, we exploited these PSs to study light-driven generation of H_2 by preparing PS–TiO_2–Pt nanocomposite materials. Both green and white light supplied by a light-emitting diode (LED) light sources were utilized to examine the effectiveness of the ZnP chromophore and bodipy-based antenna design for promoting the photoelectrochemical process. Comparisons of the UV/Vis spectra in tetrahydrofuran (THF) solutions of ZnP-dyad, YD2-*o*-C8, and Bodipy-dye before and after sonication in the presence of platinized TiO_2, were used to determine the extent of binding of the PS onto the TiO_2 particles (the corresponding spectra are displayed in Figures S20–S24.) The relatively low dye-loading values (≈40–70%) as compared to the previous reports[8a,9] were probably owing to the larger molecular size of PSs in this study. In short, the H_2 generation experiments were conducted in aqueous solutions at pH 4.0, with AA (0.5 M) serving as the hole scavenger. Similar to previous reports, GC analysis based on a methane internal standard calibration method was used to measure the amount of H_2 produced (Figure S25) at the end of the irradiation.

Plots of H_2 turnover number (TON) versus irradiation time (120 h) for ZnP-dyad, YD2-*o*-C8, and Bodipy-dye are depicted in Figure 8, and the corresponding data [TON, turnover frequency (TOF), initial TOF (TOF_i), initial activity ($Activity_i$), and apparent quantum yield (AQY_i%)] are shown in Table 3. Under green light irradiation, both ZnP-containing PSs (ZnP-dyad and YD2-*o*-C8) promoted the photocatalytic H_2 generation (>3 mL); the Bodipy-dye did not promote the reaction and its PS–TiO_2–Pt composite material rendered the same result as the bare TiO_2–Pt composite control, according to their $Activity_i$ and AQY_i%. Overall, TONs of 2600 and 2370 were obtained for ZnP-dyad and YD2-*o*-C8, respectively, but the TOF_i of YD2-*o*-C8 (60.8 h^{-1}) was almost double. The three PSs exhibited a similar pattern of activity under white-light irradiation; both the ZnP-containing PSs facilitated the light-driven H_2 generation (>16 mL) whereas Bodipy-dye remained inactive (≈2 mL) in the photocatalytic reaction. The systems with ZnP-dyad and YD2-*o*-C8 afforded high photocatalytic activity over 120 h with TONs of 12800 and 11900, respectively. Furthermore, YD2-*o*-C8 achieved

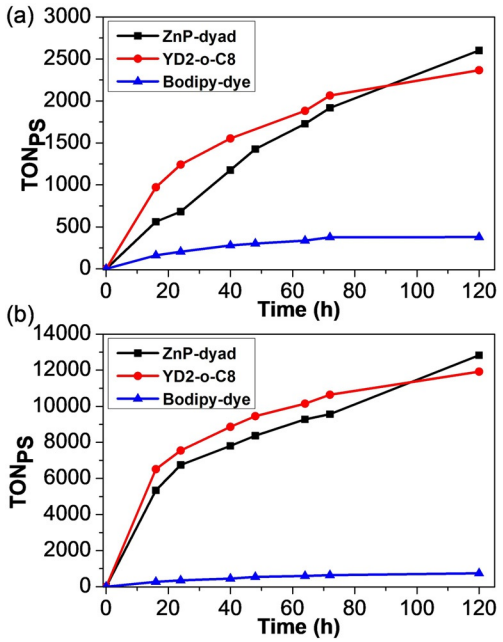

Figure 8. Photocatalytic H_2 evolution with respect to different PSs under irradiation with (a) green LED (520 nm) at 50 mW and (b) white LED (420–750 nm) at 80 mW. Each sample consisted of 5 mL of 0.5 M AA in water at pH 4.0 and 20 mg of PS–TiO_2–Pt composite material.

Table 3. Light-driven H_2 generation data with and without PSs.

Irradiation type	Dye	DL[a] [%]	H_2 [mL]	TON[b]	TOF[c] [hr^{-1}]	TOF_i[d] [hr^{-1}]	$Activity_i$[e] [$\mu mol\, g^{-1}\, h^{-1}$]	AQY_i[f] [%]
Green LED	ZnP-dyad	41.3	3.22	2600	21.7	35.1	18 100	0.464
	YD2-*o*-C8	62.8	4.45	2370	19.8	60.8	47 700	1.22
	Bodipy-dye	71.1	0.81	379	3.2	10.1	9020	0.231
	none	0	0.45[g]	–	–	–	9200	0.235
White LED	ZnP-dyad	41.5	15.95	12 800	107	334	17 3000	2.59
	YD2-*o*-C8	53.5	19.11	11 900	99.2	407	27 2000	4.07
	Bodipy-dye	71.1	1.59	744	6.2	17.1	15 200	0.228
	none	0	2.33	–	–	–	23 100	0.346

[a] Dye-loading percentage. [b] Turnover number (TON) of H_2 was calculated as the number of mole of H_2 produced divided by the number of mole of PS attached to platinized TiO_2. [c] Turnover frequency (TOF) was calculated as TON divided by the number of hours (i.e. 120 h). [d] Initial turnover frequency (TOF_i) in the first 16 h. [e] Initial photocatalytic activity ($Activity_i$) of the system was defined as the number of micromole of H_2 evolved per gram of platinum loaded per hour. [f] Initial apparent quantum yield percentage (AQY_i%) of the system. [g] 48 h instead of 120 h.

a remarkable $TOF_i > 400\ h^{-1}$ and the ZnP-dyad reached a TOF_i of 334 h^{-1}.

Under both green- and white-light irradiation, the resultant H_2 generation by the Bodipy-dye-based system was essentially the same as the control. This indicated that the dye-sensitization approach was not effective, even though the bodipy chromophore is highly light-absorbing in the 500–550 nm wavelength region. Another structurally similar bodipy-based sensitizer demonstrated poor efficiency of electron injection in another study,[26] whereas Ziessel et al. proposed that the disubstitution of long alkoxyl groups at the 4-position of bodipy chromophore through carbon–carbon triple bonds could improve the charge recombination with TiO_2.[27] According to the computational studies (Figure 4c), the HOMO and LUMO both remained at the center of Bodipy-dye chromophore and, presumably, the phenylethynylene moiety and the adjoining phenyl ring acted as an insulating layer and blocked the photoinduced electron injection into TiO_2 owing to the disconnection of π-conjugation. Therefore, even when intense green light was used to photoexcite the PS, the light-harvesting effect by the organic PS still remained minimal.

Conversely, both ZnP-containing PSs possessed a certain degree of LUMO at the anchor-adjoining phenylethynylene moiety (Figures 4a and b), ensuring an effective photoinduced electron injection into the conduction band of TiO_2 from both the ZnP-dyad and YD2-*o*-C8. As a result, the dye-sensitization approach was effective for these two PSs and the production of H_2 was realized in both cases. Based on the final TON values the two PSs generated approximately 5 times more H_2 under white-light irradiation than under green-light irradiation. Additionally, the initial TOF was 4–6 times larger under white-light illumination, even after taking into account the 60% larger intensity of the white-light LED compared to the green LED. Consequently, the significant differences in TON revealed the benefit of developing panchromatic dyes for photocatalytic reactions, especially for the solar-driven water splitting reaction and related photocatalysis.[28,29]

From the TA result, a 2.3 ps time constant was assigned for the singlet energy transfer from the bodipy unit to the ZnP moiety, comparable to those (i.e., 0.51–0.73 ps) of the reported bodipy-conjugated PtN_2S_2 PSs. In the bodipy-PtN_2S_2 systems, the bodipy-antenna was an effective energy-transfer chromophore towards the PtN_2S_2 charge-transfer moiety, increasing the H_2 production efficiency.[10b,30] Accordingly, our dyad design should make a positive contribution towards H_2 generation compared to ZnP alone. In addition, Hupp et al. reported that a similar bodipy-conjugated ZnP dyad (structure shown in Figure S29) exhibited higher incident photon-to-current efficiencies in the range of 500–550 nm as compared to another ZnP-based PS without the bodipy unit (structure shown in Figure S29), for the corresponding DSSCs.[15] In brief, the bodipy unit was shown to facilitate light-harvesting using the dyad approach, in agreement with the efficacy observed for our ZnP-dyad towards hydrogen production, which depended on the same electron injection processes as the prior DSSC study by Hupp.

On the basis of structural consideration, the ZnP-dyad was different from the push–pull type YD2-*o*-C8 PS containing a diarylamino moiety, which has been proven to provide strong electron-donating strength towards the ZnP unit in previous studies by Yeh, Diau and co-workers.[13a,b] Therefore, the electron injection step for YD2-*o*-C8 was anticipated to be faster than that of ZnP-dyad because of the strong charge pushing effect.[31] Additionally, the hole in the HOMO on YD2-*o*-C8 is localized further away from the surface of TiO_2, potentially slowing down back-transfer of electrons from the semiconductor and enhancing overall efficiency.

However, when white-light irradiation was exploited, the stronger light absorbing capability throughout the visible light region of the ZnP-dyad relative to YD2-*o*-C8 (see Figure 2) compensated for the poorer charge separation effectiveness, which led to almost the same TOF_i for these two ZnP-containing PSs.

Conclusions

ZnP-sensitized platinized TiO_2 was used for light-driven hydrogen generation from aqueous media. The absorption spectrum

of the bodipy-conjugated ZnP-dyad successfully intensified and extended the absorption throughout the visible region, filling up the weak absorption in the range of 500–550 nm of YD2-*o*-C8 and other porphyrins. Ultrafast transient absorption spectroscopy was used to determine that the time constant for the singlet energy transfer from the bodipy unit to the ZnP chromophore was 2.3 ps, supporting the possibility to utilize the energy transferred from the bodipy chromophore for effective charge separation at the interface between PS and TiO_2. However, the photocatalytic system with YD2-*o*-C8 still performed better than that of ZnP-dyad and provided a TOF_i that was almost two time higher under green-light excitation; this comparison indicated that the electronic push–pull configuration played a pivotal role for ZnP PS at the charge-separation interface. Conversely, both ZnP-containing PSs provided much higher initial TOFs and total TONs when white-light irradiation was used. This result clearly demonstrated the importance and advantage of panchromatic sensitization. A very active H_2 generation system was prepared with YD2-*o*-C8, with a TOF_i of 407 h^{-1} and TON of approximately 12000 over 120 h. Notably, this pilot study on panchromatic ZnP PSs paves the way for improving the photocatalytic system, especially in the context of solar-driven H_2 production and other related photocatalytic reactions.

Experimental Section

General

All chemical reactions were performed under an inert nitrogen atmosphere through the use of a Schlenk line. Glassware was dried in an oven prior to use. Commercially available reagents were used without purification. All the reagents for chemical synthesis were purchased from Tokyo Chemical Industry Co., Ltd (TCI), Sigma–Aldrich, Acros Organics, or Dieckmann. Solvents were dried by distillation over suitable drying agents. PS YD2-*o*-C8 was purchased from Yingkou OPV Tech New Energy Co., Ltd. All the reactions were monitored by thin-layer chromatography (TLC) with Merck pre-coated aluminum plates. Products were purified by column chromatography on silica gel (230–400 mesh) purchased from Merck.

Characterization

^1H and ^{13}C NMR spectra were measured in $CDCl_3$ or $[D_8]THF$ on a Bruker Ultra-shield 400 MHz FT-NMR spectrometer and tetramethylsilane (TMS) was used as an internal standard for calibrating the chemical shift. MALDI-TOF mass spectrometry was performed on an Autoflex Bruker MALDI-TOF system. UV/Vis absorption spectroscopy was performed on a Hewlett Packard 8453 spectrometer in dichloromethane solution at 293 K. The solution emission spectra and lifetimes of the PSs were measured on a PerkinElmer LS50B spectrophotometer at 293 K. Electrochemical measurements were conducted on a CHI 630C Electrochemical Analyzer/Workstation at a scan rate of 100 mV s^{-1}.

Preparation of platinized TiO_2

For a 0.5 wt% platinized TiO_2 sample, the addition of 40 mL methanol to 1.6 g of titanium(IV) oxide nanopowder (anatase, <25 nm particle size, 99.7% trace metals basis, Sigma–Aldrich) and 0.1 mL of H_2PtCl_6 aqueous solution (8 wt%) created a slurry, which was then subjected to radiation from a 300 W coated Hg lamp (HF300PD, EYE Lighting) under vigorous stirring for 24 h. The resulting crude product had a grayish color. Platinized TiO_2 was then retrieved by centrifugation at 3500 rpm for 5 min and washed three times with methanol. The obtained material was dried under vacuum at approximately 60 °C in darkness for 8 h.

Adsorption of photosensitizer onto platinized TiO_2

20 mg of the prepared platinized TiO_2 was added to 2.5 mL of 50 μM PS THF solution, the mixture was then sonicated for 30 min. The solution lost color gradually while the solid became pink or dark-green. The dye-loaded solid was then retrieved by centrifugation at 3500 rpm for 5 min. The supernatant layer solvent was removed carefully using a dropper and the pellet at the bottom was dried under vacuum for 2—3 h in darkness. The whole dried pellet was directly utilized without further characterization in the photocatalytic reaction mixture for one photolysis experiment.
The dye loading percentage, DL%, for each PS was estimated by comparing the absorbance value of the absorption peak with the highest ε before and after the dye adsorption (Table 3). The corresponding UV/Vis spectra for ZnP-dyad, YD2-*o*-C8, and Bodipy-dye are shown in Figures S20–S24.

Light-driven hydrogen production studies

The photocatalytic reactions were performed in 5 mL aqueous AA (0.5 M) solution at pH 4.0 with AA serving as the sacrificial electron donor (SED; AA was selected in our system because of its relationship between the pH value and H_2-evolving activity has recently been studied in detail and the redox chemistry is also well-known[32]). A 25 mL pear-shaped flask was placed above stirrers at 19 °C and the flask was sealed with rubber septa. The photocatalytic reaction mixture with a stir bar was then purged with a mixture of gas containing argon/methane (80:20 mol%) for 15 min. The methane present in the gas mixture served as an internal standard for GC analysis at the end of each experiment. The reaction mixture was steadily stirred and continuously radiated from the bottom with green ($\approx$520 nm) and white light-emitting diodes (420–750 nm) inside a just-fit container, which blocked the stray light from the environment. The light power was measured with a thermal sensor (Model: BIM-7203-0100F) and power meter (Model: BIM-7001; Hangzhou Brolight Technology Co., Ltd.), and estimated to be approximately 50 mW (green light) and 80 mW (white light) for each reaction mixture. At the end of the experiment, the headspaces of the flasks were characterized by GC to examine the amount of hydrogen produced. The amounts of hydrogen evolved were determined by GC (Shimadzu GC-8A with a molecular sieve 5 Å column and TCD detector) at the end of the radiation period and were quantified using a calibration plot of the integrated amount of hydrogen relative to the methane (Figure S25). During the radiation, GC samples were taken at different time points. The LED radiation was assumed to be monochromatic at the emission intensity maximum (520 nm for green light; 556 nm for white light) and the corresponding apparent quantum yield values for each photosensitizer were estimated according to the equation shown below.

$$\mathrm{AQY}\ (\%) = \frac{\text{rate of } H_2 \text{ production} \times 2}{\text{rate of incident photons}} \times 100\,\%$$

Synthetic procedures of intermediates and PSs

Compound 1: 3-Ethyl-2,4-dimethyl-1*H*-pyrrole (950 mg, 7.72 mmol), 4-iodobenzoyl chloride (1.03 g, 3.87 mmol), and dry CH_2Cl_2 (50 mL) were stirred in the dark overnight at 25 °C. NEt_3 (2.5 mL) was then added. After 10 min, boron trifluoride etherate (2.5 mL, 20.13 mmol) was introduced and the reaction mixture was stirred for 1 h. The crude mixture was purified by column chromatography on silica gel, and the product band was eluted with CH_2Cl_2/hexane (1:1, v/v) as an eluent. Recrystallization of the product was performed with CH_2Cl_2/diethyl ether to yield compound **1** as a red solid (413 mg, 0.79 mmol, 20%). ^{1}H NMR ($CDCl_3$, 400 MHz): δ = 7.85–7.82 (m, 2H, Ar), 7.04 (d, 2H, J = 8.4 Hz, Ar), 2.53 (s, 6H, alkyl), 2.30 (q, 4H, J = 7.6 Hz, alkyl), 1.32 (s, 6H, alkyl), 0.98 ppm (t, 6H, J = 7.6 Hz, alkyl); ^{13}C NMR (100 MHz, $CDCl_3$): δ = 154.15, 138.52, 138.25, 138.17, 135.38, 133.03, 130.49, 130.29, 94.51 (Ar), 17.08, 14.64, 12.56, 11.99 ppm (alkyl). HRMS (MALDI-TOF, *m/z*): [M^+] 506.1205; calcd for ($C_{23}H_{26}BF_2IN_2$) 506.1202.

Compound 2: A mixture of compound 1 (60 mg, 0.119 mmol), trimethylsilylacetylene (0.05 mL), $Pd(PPh_3)_2Cl_2$ (7 mg, 0.009 mmol), and CuI (2 mg, 0.009 mmol) in a mixture of THF/NEt_3 (10/1, 22 mL) was heated to reflux under a nitrogen atmosphere overnight. The solvent was removed under reduced pressure. The residue was purified by column chromatography on silica gel using a 1:2 mixture of CH_2Cl_2 and hexane as eluent to afford compound **2** (52 mg, 0.088 mmol, 74%) as a red solid. ^{1}H NMR ($CDCl_3$, 400 MHz): δ = 7.60 (d, 2H, J = 8.4 Hz, Ar), 7.24 (d, 2H, J = 8.4 Hz, Ar), 2.53 (s, 6H, alkyl), 2.30 (q, 4H, J = 7.6 Hz, alkyl), 1.29 (s, 6H, alkyl), 0.98 (t, 6H, J = 7.6 Hz, alkyl), 0.29 ppm (s, 9H, $Si(CH_3)_3$); ^{13}C NMR (100 MHz, $CDCl_3$): δ = 154.01, 139.20, 138.23, 136.08, 132.92, 132.65, 130.49, 128.38 (Ar), 104.36, 95.61 (C≡C), 17.07, 14.64, 12.54, 11.91 (alkyl), −0.07 ppm ($Si(CH_3)_3$). HRMS (MALDI-TOF, *m/z*): [M^+] 592.2420; calcd for ($C_{30}H_{41}BCl_2F_2N_2OSi$) 592.2426.

Compound 3: To a flask containing the ethynyl precursor (52 mg, 0.109 mmol) and K_2CO_3 (151 mg, 1.09 mmol) was added 22 mL of CH_2Cl_2/CH_3OH (10:1, v/v). The solution was allowed to stir at room temperature for 3 h. The solvents were then removed by evaporation under reduced pressure, and the residue was extracted with CH_2Cl_2 and washed with water (3×20 mL). The organic layer was evaporated under reduced pressure and purified by column chromatography on silica gel using a mixture of hexane/CH_2Cl_2 (1:1, v/v) as eluent to obtain a red solid (24 mg, 0.059 mmol, 54%). ^{1}H NMR ($CDCl_3$, 400 MHz): δ = 7.63–7.61 (m, 2H, Ar), 7.28–7.26 (m, 2H, Ar), 3.19 (s, 1H, C≡C–H), 2.53 (s, 6H, alkyl), 2.30 (q, 4H, J = 7.6 Hz, alkyl), 1.30 (s, 6H, alkyl), 0.98 ppm (t, 6H, J = 7.6 Hz, alkyl); ^{13}C NMR (100 MHz, $CDCl_3$): δ = 154.09, 139.01, 138.20, 136.45, 132.97, 132.79, 130.48, 128.51, 122.67 (Ar), 83.03, 78.43 (C≡C), 17.08, 14.64, 12.55, 11.89 ppm (alkyl). HRMS (MALDI-TOF, *m/z*): [M^+] 404.2239; calcd for ($C_{25}H_{27}BF_2N_2$) 404.2235.

ZnP-dyad: Protected diethynyl precursor ZnP (54 mg, 0.039) was dissolved in 20 mL THF, the solution was then cooled in an ice bath followed by the addition of tetra(*n*-butyl)ammonium fluoride (1 M in THF, 0.39 mL, 0.386 mmol). After stirring for 1 h, the solution was evaporated under reduced pressure. The resulting residues were extracted with CH_2Cl_2 and washed with water (3×20 mL). The solvent was evaporated under reduced pressure and the residue was redissolved in a 25 mL mixture of THF/NEt_3 (2:3, v/v) and subsequently cooled in an ice-bath. To this reaction mixture, compound 1 (20 mg, 0.039 mmol), 4-iodobenzoic acid (10 mg, 0.039 mmol), $Pd_2(dba)_3$ (2 mg, 0.002 mmol), PPh_3 (1 mg, 0.04 mmol), and CuI (1 mg, 0.002 mmol) were added. The reaction mixture was stirred at 0 °C for 30 min and then refluxed overnight (the temperature was increased slowly). After the solvent was removed under reduced pressure, the residue was purified by column chromatography on silica gel with pure CH_2Cl_2, and the product band was eluted with CH_2Cl_2/CH_3OH (19:1, v/v) to afford a dark solid. This solid was further purified by precipitation using CH_2Cl_2/hexane and the precipitate was dried under vacuum to yield the PS ZnP-dyad (32 mg, 0.020 mmol, 51%) as a dark solid. ^{1}H NMR ($CDCl_3$, 400 MHz): δ = 9.72 (d, 2H, J = 4.8 Hz, Ar), 9.67 (d, 2H, J = 4.8 Hz, Ar), 8.91–8.90 (m, 4H, Ar), 8.21 (d, 2H, J = 8 Hz, Ar), 8.14 (d, 2H, J = 8.4 Hz, Ar), 8.06 (d, 2H, J = 8.4 Hz, Ar), 7.75–7.71 (m, 2H, Ar), 7.49 (d, 2H, J = 8 Hz, Ar), 7.03 (d, 4H, J = 8.4 Hz, Ar), 3.88 (t, 8H, J = 6.4 Hz, alkyl), 2.58 (s, 6H, alkyl), 2.37–2.34 (m, 4H, alkyl), 1.26 (s, 6H, alkyl), 1.05–0.97 (m, 14H, alkyl), 0.85–0.80 (m, 8H, alkyl), 0.66–0.49 (m, 8H, alkyl), 0.45–0.38 ppm (m, 36H, alkyl); ^{13}C NMR (100 MHz, $CDCl_3$): δ = 159.86 (COOH), 154.01, 151.68, 151.53, 150.75, 139.58, 138.42, 135.56, 132.98, 132.19, 132.05, 130.71, 130.52, 129.96, 128.76, 125.17, 120.66, 115.65, 105.18 (Ar), 99.99, 99.31, 95.11, 94.60 (C≡C), 68.61, 31.39, 29.71, 29.66, 29.61, 29.46, 29.37, 29.33, 29.10, 28.73, 28.65, 28.58, 27.21, 25.26, 22.29, 17.13, 14.67, 13.85, 12.59, 12.06 ppm (alkyl). HRMS (MALDI-TOF, *m/z*): [(M+H)$^+$] 1584.8108; calcd for ($C_{98}H_{114}BF_2N_6O_6Zn$) 1584.8186.

Bodipy-dye: A mixture of compound 3 (24 mg, 0.059 mmol), 4-iodobenzoic acid (13 mg, 0.050 mmol), $Pd_2(dba)_3$ (3 mg, 0.003 mmol), PPh_3 (1.5 mg, 0.06 mmol), and CuI (1 mg, 0.003 mmol) in a mixture of THF/NEt_3 (20/1, 21 mL) was heated to reflux under a nitrogen atmosphere overnight. The solvent was removed under reduced pressure. After the removal of the solvent, the impurities were removed by column chromatography on silica gel using pure CH_2Cl_2, and the product band was eluted with CH_2Cl_2/CH_3OH (10:1, v/v) to afford the photosensitizer Bodipy-dye (24 mg, 0.046 mmol, 78%) as a red solid. ^{1}H NMR ([D_8]THF, 400 MHz): δ = 8.04 (d, 2H, J = 6.8 Hz, Ar), 7.73 (d, 2H, J = 8.4 Hz, Ar), 7.64 (d, 2H, J = 7.6 Hz, Ar), 7.41 (d, 2H, J = 8 Hz, Ar), 2.49 (s, 6H, alkyl), 2.34 (q, 4H, J = 7.6 Hz, alkyl), 1.38 (s, 6H, alkyl), 0.99 ppm (t, 6H, J = 7.6 Hz, alkyl); ^{13}C NMR (100 MHz, [D_8]THF): δ = 153.74, 139.53, 137.56, 136.47, 132.56, 132.21, 131.24, 130.39, 129.66, 128.89, 127.07, 123.51 (Ar), 91.04, 89.57 (C≡C), 16.69, 14.00, 11.59, 11.15 ppm (alkyl). HRMS (MALDI-TOF, *m/z*): [M^+] 524.2489; calcd for ($C_{32}H_{31}BF_2N_2O_2$) 524.2447.

Transient absorption

A regeneratively amplified titanium:sapphire laser (Spectra-Physics Spitfire) was used to produce femtosecond laser pulses at a 1 kHz repetition rate. The pump pulse was produced from a home-built noncollinear optical parametric amplifier (NOPA) centered at three different wavelengths of 470, 520, and 650 nm with a pulse energy of 100 nJ per pulse and a bandwidth of 14, 11, and 40 nm, respectively.[33] A mechanical chopper was used to block every other pump pulse. The probe beam was created by focusing of the fundamental 800 nm beam through either a sapphire crystal to produce a white light continuum spanning 425–950 nm or through calcium fluoride (CaF_2) giving a continuum from 350–650 nm. The probe was dispersed by a grating spectrograph (Acton, 300 mm fl, 150gr mm^{-1}) before reaching the CCD camera (Princeton Instruments, Pixis 100BR). The white light spectrum was filtered using a dye solution (NIR800A, QCR Solutions Corp) to block residual 800 nm light from entering the spectrograph during sample collection and a 780 nm long pass when collecting signals in the near-infrared (NIR). Solution samples were prepared in a 2 mm fused-silica cuvette and diluted to an absorbance of approximately 0.1–0.7 and the cuvettes were translated vertically at approximately

2 mm s^{-1} to refresh the illuminated sample. The TA signal was collected using both a parallel and perpendicular pump to probe the polarizations, with the isotropic (magic angle) signal calculated by:

$$\Delta A_{Iso} = \frac{(\Delta A_{||} + 2\Delta A_{\perp})}{3} \quad (2)$$

Kinetic data was fit to a series of exponentials with varying amplitudes, convoluted with a Gaussian instrument response function that was established by the pump-probe cross-correlation. Cross-correlations (XC) were determined from Optical Kerr Effect (OKE) signals obtained when the pump and probe were overlapped on a 1 mm glass slide. OKE signals were averaged over all wavelengths of interest, giving values of 100, 60, and 50 fs for excitation wavelengths of 470, 520, and 650 nm, respectively.

Computational studies

DFT calculations and time-dependent DFT (TD-DFT)[34] calculations provide useful information about the nature of electronic ground states and excited states, respectively. Both DFT and TD-DFT calculations were performed by using the Gaussian 09 package.[35] The B3LYP[36] hybrid functional with 20% Hatree-Fock exchange and LC-wPBE functional were used. The 6-31G(d,p) basis set was used for C, H, B, F, N, O, S, and Zn. The optimized geometries for ZnP-dyad, YD2-*o*-C8, and Bodipy-dye were confirmed with all real frequencies.

Acknowledgements

C.-L.H. thanks the Hong Kong Research Grants Council (PolyU 123021/17P), National Natural Science Foundation of China (21504074), the Science, Technology and Innovation Committee of Shenzhen Municipality (JCYJ20160531193836532), and the Hong Kong Polytechnic University (1-BE0Q) for their financial support. M.F.M., D.W.M., and R.E. were supported by a grant from the U.S. National Science Foundation's Chemical Catalysis division under Collaborative Research Grant CHE- 1566080. We are thankful to Jacob Shelton and Kathryn Knowles at the University of Rochester for their assistance with the diffuse reflectance measurements.

Conflict of interest

The authors declare no conflict of interest.

Keywords: hydrogen production · photocatalysis · photosensitizer · transient absorption · Zn^{II} porphyrin

[1] S. Chu, A. Majumdar, *Nature* **2012**, *488*, 294 – 303.
[2] a) J. Lelieveld, J. S. Evans, M. Fnais, D. Giannadaki, A. Pozzer, *Nature* **2015**, *525*, 367 – 371; b) C. McGlade, P. Ekins, *Nature* **2015**, *517*, 187 – 190.
[3] a) T. Hisatomi, J. Kubota, K. Domen, *Chem. Soc. Rev.* **2014**, *43*, 7520 – 7535; b) N. S. Lewis, D. G. Nocera, *Proc. Natl. Acad. Sci. USA* **2006**, *103*, 15729 – 15735; c) H. Ahmad, S. K. Kamarudin, L. J. Minggu, M. Kassim, *Renewable Sustainable Energy Rev.* **2015**, *43*, 599 – 610; d) Z. Li, W. Luo, M. Zhang, J. Feng, Z. Zou, *Energy Environ. Sci.* **2013**, *6*, 347 – 370.
[4] P. V. Kamat, J. Bisquert, *J. Phys. Chem. C* **2013**, *117*, 14873 – 14875.
[5] G. Centi, S. Perathoner, *Green carbon dioxide: Advances in CO2 utilization*, Wiley, **2014**.
[6] a) A. J. Bard, M. A. Fox, *Acc. Chem. Res.* **1995**, *28*, 141 – 145; b) L.-Z. Wu, B. Chen, Z.-J. Li, C.-H. Tung, *Acc. Chem. Res.* **2014**, *47*, 2177 – 2185; c) J. J. Concepcion, J. W. Jurss, M. K. Brennaman, P. G. Hoertz, A. O. T. Patrocinio, N. Y. Murakami Iha, J. L. Templeton, T. J. Meyer, *Acc. Chem. Res.* **2009**, *42*, 1954 – 1965.
[7] W. T. Eckenhoff, R. Eisenberg, *Dalton Trans.* **2012**, *41*, 13004 – 13021.
[8] a) P.-Y. Ho, Y. Wang, S.-C. Yiu, W.-H. Yu, C.-L. Ho, S. Huang, *Org. Lett.* **2017**, *19*, 1048 – 1051; b) W. J. Youngblood, S. H. Lee, Y. Kobayashi, E. A. Hernandez-Pagan, P. G. Hoertz, T. A. Moore, A. L. Moore, D. Gust, T. E. Mallouk, *J. Am. Chem. Soc.* **2009**, *131*, 926 – 927; c) L. Li, L. Duan, Y. Xu, M. Gorlov, A. Hagfeldt, L. Sun, *Chem. Commun.* **2010**, *46*, 7307 – 7309; d) E. D. Cline, S. E. Adamson, S. Bernhard, *Inorg. Chem.* **2008**, *47*, 10378 – 10388; e) P. Du, K. Knowles, R. Eisenberg, *J. Am. Chem. Soc.* **2008**, *130*, 12576 – 12577; f) P. Jarosz, P. Du, J. Schneider, S.-H. Lee, D. McCamant, R. Eisenberg, *Inorg. Chem.* **2009**, *48*, 9653 – 9663; g) P. N. Curtin, L. L. Tinker, C. M. Burgess, E. D. Cline, S. Bernhard, *Inorg. Chem.* **2009**, *48*, 10498 – 10506.
[9] P.-Y. Ho, B. Zheng, D. Mark, W.-Y. Wong, D. W. McCamant, R. Eisenberg, *Inorg. Chem.* **2016**, *55*, 8348 – 8358.
[10] a) G. J. Meyer, *Proc. Natl. Acad. Sci. USA* **2015**, *112*, 9146 – 9147; b) B. Zheng, R. P. Sabatini, W.-F. Fu, M.-S. Eum, W. W. Brennessel, L. Wang, D. W. McCamant, R. Eisenberg, *Proc. Natl. Acad. Sci. USA* **2015**, *112*, E3987 – E3996.
[11] a) W. M. Campbell, K. W. Jolley, P. Wagner, K. Wagner, P. J. Walsh, K. C. Gordon, L. Schmidt-Mende, M. K. Nazeeruddin, Q. Wang, M. Grätzel, D. L. Officer, *J. Phys. Chem. C* **2007**, *111*, 11760 – 11762; b) R. C. Hardison, *Proc. Natl. Acad. Sci. USA* **1996**, *93*, 5675 – 5679.
[12] a) M. Gouterman, *J. Mol. Spectrosc.* **1961**, *6*, 138 – 163; b) T. Hashimoto, Y.-K. Choe, H. Nakano, K. Hirao, *J. Phys. Chem. A* **1999**, *103*, 1894 – 1904; c) X. Huang, K. Nakanishi, N. Berova, *Chirality* **2000**, *12*, 237 – 255.
[13] a) C.-W. Lee, H.-P. Lu, C.-M. Lan, Y.-L. Huang, Y.-R. Liang, W.-N. Yen, Y.-C. Liu, Y.-S. Lin, E. W.-G. Diau, C.-Y. Yeh, *Chem. Eur. J.* **2009**, *15*, 1403 – 1412; b) S.-L. Wu, H.-P. Lu, H.-T. Yu, S.-H. Chuang, C.-L. Chiu, C.-W. Lee, E. W.-G. Diau, C.-Y. Yeh, *Energy Environ. Sci.* **2010**, *3*, 949 – 955; c) C.-P. Hsieh, H.-P. Lu, C.-L. Chiu, C.-W. Lee, S.-H. Chuang, C.-L. Mai, W.-N. Yen, S.-J. Hsu, E. W.-G. Diau, C.-Y. Yeh, *J. Mater. Chem.* **2010**, *20*, 1127 – 1134.
[14] a) A. Yella, H.-W. Lee, H. N. Tsao, C. Yi, A. K. Chandiran, M. K. Nazeeruddin, E. W.-G. Diau, C.-Y. Yeh, S. M. Zakeeruddin, M. Grätzel, *Science* **2011**, *334*, 629 – 634; b) H.-P. Wu, Z.-W. Ou, T.-Y. Pan, C.-M. Lan, W.-K. Huang, H.-W. Lee, N. M. Reddy, C.-T. Chen, W.-S. Chao, C.-Y. Yeh, E. W.-G. Diau, *Energy Environ. Sci.* **2012**, *5*, 9843 – 9848; c) T. Ripolles-Sanchis, B.-C. Guo, H.-P. Wu, T.-Y. Pan, H.-W. Lee, S. R. Raga, F. Fabregat-Santiago, J. Bisquert, C.-Y. Yeh, E. W.-G. Diau, *Chem. Commun.* **2012**, *48*, 4368 – 4370; d) M. Urbani, M. Grätzel, M. K. Nazeeruddin, T. Torres, *Chem. Rev.* **2014**, *114*, 12330 – 12396.
[15] C. Y. Lee, J. T. Hupp, *Langmuir* **2010**, *26*, 3760 – 3765.
[16] a) A. Burghart, H. Kim, M. B. Welch, L. H. Thoresen, J. Reibenspies, K. Burgess, F. Bergström, L. B. Å. Johansson, *J. Org. Chem.* **1999**, *64*, 7813 – 7819; b) Y.-C. Liu, H.-H. Chou, F.-Y. Ho, H.-J. Wei, T.-C. Wei, C.-Y. Yeh, *J. Mater. Chem. A* **2016**, *4*, 11878 – 11887.
[17] J. Karolin, L. B. A. Johansson, L. Strandberg, T. Ny, *J. Am. Chem. Soc.* **1994**, *116*, 7801 – 7806.
[18] a) M. R. Topka, P. H. Dinolfo, *ACS Appl. Mater. Interfaces* **2015**, *7*, 8053 – 8060; b) M. T. Whited, P. I. Djurovich, S. T. Roberts, A. C. Durrell, C. W. Schlenker, S. E. Bradforth, M. E. Thompson, *J. Am. Chem. Soc.* **2011**, *133*, 88 – 96; c) M. J. Leonardi, M. R. Topka, P. H. Dinolfo, *Inorg. Chem.* **2012**, *51*, 13114 – 13122.
[19] M. Galletta, F. Puntoriero, S. Campagna, C. Chiorboli, M. Quesada, S. Goeb, R. Ziessel, *J. Phys. Chem. A* **2006**, *110*, 4348 – 4358.
[20] X. Li, J. Yu, J. Low, Y. Fang, J. Xiao, X. Chen, *J. Mater. Chem. A* **2015**, *3*, 2485 – 2534.
[21] I. Chung, B. Lee, J. He, R. P. H. Chang, M. G. Kanatzidis, *Nature* **2012**, *485*, 486 – 489.
[22] S. A. Haque, E. Palomares, B. M. Cho, A. N. M. Green, N. Hirata, D. R. Klug, J. R. Durrant, *J. Am. Chem. Soc.* **2005**, *127*, 3456 – 3462.
[23] T. Bessho, E. Yoneda, J.-H. Yum, M. Guglielmi, I. Tavernelli, H. Imai, U. Rothlisberger, M. K. Nazeeruddin, M. Grätzel, *J. Am. Chem. Soc.* **2009**, *131*, 5930 – 5934.
[24] a) H. Choi, C. Baik, S. O. Kang, J. Ko, M.-S. Kang, M. K. Nazeeruddin, M. Grätzel, *Angew. Chem. Int. Ed.* **2008**, *47*, 327 – 330; *Angew. Chem.* **2008**, *120*, 333 – 336; b) A. Orbelli Biroli, F. Tessore, M. Pizzotti, C. Biaggi, R.

Ugo, S. Caramori, A. Aliprandi, C. A. Bignozzi, F. De Angelis, G. Giorgi, E. Licandro, E. Longhi, *J. Phys. Chem. C* **2011**, *115*, 23170 – 23182.
[25] M. R. di Nunzio, B. Cohen, S. Pandey, S. Hayse, G. Piani, A. Douhal, *J. Phys. Chem. C* **2014**, *118*, 11365 – 11376.
[26] M. Shrestha, L. Si, C.-W. Chang, H. He, A. Sykes, C.-Y. Lin, E. W.-G. Diau, *J. Phys. Chem. C* **2012**, *116*, 10451 – 10460.
[27] C. Qin, A. Mirloup, N. Leclerc, A. Islam, A. El-Shafei, L. Han, R. Ziessel, *Adv. Energy Mater.* **2014**, *4*, 1400085.
[28] a) X. Zhang, T. Peng, L. Yu, R. Li, Q. Li, Z. Li, *ACS Catal.* **2015**, *5*, 504 – 510; b) X. Zhang, L. Yu, C. Zhuang, T. Peng, R. Li, X. Li, *RSC Adv.* **2013**, *3*, 14363 – 14370; c) X. Zhang, B. Peng, T. Peng, L. Yu, R. Li, J. Zhang, *J. Power Sources* **2015**, *298*, 30 – 37.
[29] J. Park, G. Viscardi, C. Barolo, N. Barbero, *Chimia* **2013**, *67*, 129 – 135.
[30] R. P. Sabatini, B. Zheng, W.-F. Fu, D. J. Mark, M. F. Mark, E. A. Hillenbrand, R. Eisenberg, D. W. McCamant, *J. Phys. Chem. A* **2014**, *118*, 10663 – 10672.
[31] P. Piatkowski, C. Martin, M. R. di Nunzio, B. Cohen, S. Pandey, S. Hayse, A. Douhal, *J. Phys. Chem. C* **2014**, *118*, 29674 – 29687.
[32] M. Natali, *ACS Catal.* **2017**, *7*, 1330 – 1339.
[33] a) G. Cerullo, M. Nisoli, S. Stagira, S. De Silvestri, *Opt. Lett.* **1998**, *23*, 1283 – 1285; b) G. Cerullo, S. D. Silvestri, *Rev. Sci. Instrum.* **2003**, *74*, 1 – 18.
[34] M. A. L. Marques, E. K. U. Gross, *Annu. Rev. Phys. Chem.* **2004**, *55*, 427 – 455.
[35] Gaussian 09, Revision D.01, M. J. Frisch, G. W. Trucks, H. B. Schlegel, G. E. Scuseria, M. A. Robb, J. R. Cheeseman, G. Scalmani, V. Barone, B. Mennucci, G. A. Petersson, H. Nakatsuji, M. Caricato, X. Li, H. P. Hratchian, A. F. Izmaylov, J. Bloino, G. Zheng, J. L. Sonnenberg, M. Hada, M. Ehara, K. Toyota, R. Fukuda, J. Hasegawa, M. Ishida, T. Nakajima, Y. Honda, O. Kitao, H. Nakai, T. Vreven, J. A. Montgomery, Jr., J. E. Peralta, F. Ogliaro, M. J. Bearpark, J. Heyd, E. N. Brothers, K. N. Kudin, V. N. Staroverov, R. Kobayashi, J. Normand, K. Raghavachari, A. P. Rendell, J. C. Burant, S. S. Iyengar, J. Tomasi, M. Cossi, N. Rega, N. J. Millam, M. Klene, J. E. Knox, J. B. Cross, V. Bakken, C. Adamo, J. Jaramillo, R. Gomperts, R. E. Stratmann, O. Yazyev, A. J. Austin, R. Cammi, C. Pomelli, J. W. Ochterski, R. L. Martin, K. Morokuma, V. G. Zakrzewski, G. A. Voth, P. Salvador, J. J. Dannenberg, S. Dapprich, A. D. Daniels, Ö. Farkas, J. B. Foresman, J. V. Ortiz, J. Cioslowski, D. J. Fox, Gaussian, Inc., Wallingford CT, **2013**.
[36] a) A. D. Becke, *Phys. Rev. A* **1988**, *38*, 3098 – 3100; b) C. Lee, W. Yang, R. G. Parr, *Phys. Rev. B* **1988**, *37*, 785 – 789; c) P. J. Stephens, F. J. Devlin, C. F. Chabalowski, M. J. Frisch, *J. Phys. Chem.* **1994**, *98*, 11623 – 11627.

Manuscript received: June 5, 2018
Accepted manuscript online: June 19, 2018
Version of record online: July 25, 2018